Calculating Two-Dimensional Spectra with the Mixed Quantum-Classical Ehrenfest Method

ARTICLE *in* THE JOURNAL OF PHYSICAL CHEMISTRY A · JANUARY 2013

Impact Factor: 2.69 · DOI: 10.1021/jp311668r · Source: PubMed

4 AUTHORS, INCLUDING:

Arend G. Dijkstra
Max Planck Institute for the Structure and Dyn…
27 PUBLICATIONS **451** CITATIONS
SEE PROFILE

Thomas La Cour Jansen
University of Groningen
78 PUBLICATIONS **1,720** CITATIONS
SEE PROFILE

THE JOURNAL OF PHYSICAL CHEMISTRY A

Article

pubs.acs.org/JPCA

Calculating Two-Dimensional Spectra with the Mixed Quantum-Classical Ehrenfest Method

C. P. van der Vegte,*[,†] A. G. Dijkstra,*[,‡] J. Knoester,*[,†] and T. L. C. Jansen*[,†]

[†]Zernike Institute for Advanced Materials, University of Groningen, Nijenborgh 4, 9747 AG Groningen, The Netherlands

[‡]Department of Chemistry, Massachusetts Institute of Technology, 77 Massachusetts Avenue, Cambridge, Massachusetts 02139, United States

ABSTRACT: We present a mixed quantum-classical simulation approach to calculate two-dimensional spectra of coupled two-level electronic model systems. We include the change in potential energy of the classical system due to transitions in the quantum system using the Ehrenfest method. We study how this feedback of the quantum system on the classical system influences the shape of two-dimensional spectra. We show that the feedback leads to the expected Stokes shift of the energy levels in the quantum system. This subsequently leads to changes in the population transfer between quantum sites, which in turn influence the intensities of the peaks in two-dimensional spectra. The obtained spectra are compared with spectra calculated using the Hierarchical Equations of Motion method which is exact. While the spectra match perfectly for short waiting times, clear differences are found for longer waiting times. This is attributed to a violation of detailed balance between the quantum states in the Ehrenfest method. The energy of the total quantum-classical system however does obey a Boltzmann distribution, when coupled to a stochastic heat bath.

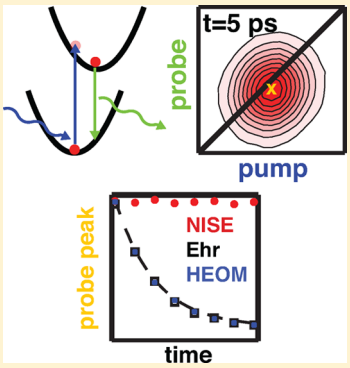

INTRODUCTION

Two-dimensional spectroscopy has proven to be a powerful tool for investigating and characterizing chemical and physical processes in molecular systems down to the femtosecond time scale.[1−5] It has been applied successfully to processes like proton transfer[6−8] and hydrogen bond breaking.[9,10] The cross peaks in two-dimensional spectra are determined by the couplings in the molecular system and are sensitive to population transfer between different eigenstates. This allows one to follow vibrational[11−14] and electronic[2,15−17] population transfer in complex molecular systems. Measured two-dimensional spectra are, however, difficult to interpret. Therefore, theoretical models and simulations are crucial for a better understanding of the measured spectra. For example, in the first electronic two-dimensional spectra measured for light harvesting complexes[2] oscillations were observed. This led to the idea that coherent transport may play a role in biological systems. The observed oscillations may indeed arise from coherent population transfer, but underdamped vibrations in the environment and the coherent nature of the excitations may lead to oscillations as well. Theoretical models and simulations are needed to disentangle these effects. Here we will propose a new simulation method that allows a general treatment of most of the physical phenomena that determine the spectral shapes.

Two-dimensional spectroscopy is typically performed in solution. The chromophores are influenced by fluctuations of the solvent environment and vice versa. A full quantum description of such systems is not feasible because of the large number of degrees of freedom involved. Therefore several approximate schemes have been applied. If the temperature is sufficiently high, a complete classical treatment may be valid;[18] however, at room temperature this neither applies to vibrational nor to electronic spectroscopy. Alternatively, one can treat the environment classically using molecular dynamics simulations and use a quantum description of the chromophores. For this to be valid the thermal energy (k_BT) should be high compared to the energy difference between states of the degrees of freedom treated classically. This approach has been applied quite successfully in the so-called numerical integration of the Schrödinger equation (NISE) implementation.[19−21] When a chromophore is excited, the charge density of the molecule changes. This subsequently changes the potential the environmental molecules feel. This feedback of the chromophores, which are treated quantum mechanically, on the classical environment, is not included in the NISE method, since it assumes a ground-state classical path approximation. Giving up an explicit description of the bath degrees of freedom for a stochastic description, one can apply Redfield theory[22] to calculate the two-dimensional spectra.[23] While this is a perturbative approximation it is valid at low temperatures. Similarly the Pauli Master equation can be used.[24] As both these methods rely on perturbation theory, they may fail if the quantum levels are degenerate or close to degenerate. Furthermore, these perturbative approaches treat the environment as a stochastic bath and they assume Gaussian dynamics. This approximation has been found not to apply for a light harvesting system at room temperature,[25] and is known to

Special Issue: Prof. John C. Wright Festschrift

Received: November 27, 2012
Revised: January 25, 2013
Published: January 29, 2013

affect the two-dimensional spectral lineshapes.[9,26,27] Likewise, nonperturbative Stochastic Liouville Equation type approaches rely on a correlation function-based description of the bath as well.[28] A quite general mixed quantum-classical Liouville approach has been implemented for single chromophores.[29−32] Finally, the hierarchical equations of motion (HEOM) provide a way to calculate the exact two-dimensional spectra, but so far this method only has been implemented for an environment with Gaussian motion.[33−35] Furthermore this method is rather expensive computationally. The method does, however, provide an important benchmark for other methods.

Other ways exist to treat the dynamics of coupled chromophores in complex environments. These have thus far not been applied to simulate two-dimensional spectra. Among such methods are the Lindblad equations,[36] the scaled coupling method,[37] the fewest-switches surface hopping method,[38] and Ehrenfest dynamics.[39,40] In this paper we will develop the machinery to calculate two-dimensional spectra using the latter method. This method is very similar to the NISE method but differs from it by including the feedback of the quantum system on the classical environment using a mean field approximation. Like NISE, this approach should be applicable to a wide range of situations including problems with underdamped vibrations in the environment, non-Gaussian dynamics,[25,26] and non-Condon effects,[41] but, in contrast to NISE, it includes the Stokes shift.

We will study the influence of the quantum force on the environment resulting from transitions in the quantum system on the shape of two-dimensional spectra, using the Ehrenfest method mentioned above. The method for calculating two-dimensional electronic spectra including the feedback of the quantum system will be explained in section II. If the feedback term is neglected, this method reduces to the NISE method.[19,21] In section III the simulated two-dimensional spectra excluding and including the feedback will be compared. As a benchmark we compare the obtained spectra with spectra calculated using the HEOM. This restricts us to using Gaussian motion, which can be described with HEOM. For a single two-level system we show that the feedback results in a Stokes shift of its transition energy. The Ehrenfest and HEOM method give excellent correspondence for the single chromophore. For two coupled two-level systems the Stokes shift alters the population transfer between the one-quantum eigenstates and influences the peak positions and growth of the cross-peaks when the time between the pump and probe pulses, also denoted the waiting time, is increased. The Ehrenfest method gives an improved behavior with respect to the NISE method but does not reproduce the HEOM method if the thermal energy is small compared to the energy difference between the eigenstates. We study the equilibrium limits of the Ehrenfest method and show that the total energy of the quantum-classical system obeys a Boltzmann distribution; however, the Ehrenfest method does not result in a Boltzmann distribution in the quantum subsystem solely if the energy difference between two chromophores is nonzero as previously discussed by Tully et al.[42] The formalism presented can easily be extended to coupled three-level systems needed in the calculation of two-dimensional infrared spectra. Finally, we will present our conclusions in section IV.

THEORY

Ehrenfest Method for Calculating Two-Dimensional Spectra. We treat the part of the sample that directly interacts with the applied laser fields quantum mechanically (the electronic quantum system) and the part of the sample not interacting with the light, but strongly interacting with the quantum system classically (the classical system). All other degrees of freedom are treated as a weakly interacting stochastic bath. The total Hamiltonian of the system can then be written as

$$H(t) = H_{\mathrm{Q}}(t) + H_{\mathrm{C}}(t) + H_{\mathrm{Q-C}}(t) + H_{\mathrm{light}}(t) \tag{1}$$

where H_{Q} and H_{C} denote the Hamiltonians of the quantum system and classical system, respectively, $H_{\mathrm{Q-C}}$ describes the interaction between the two subsystems, and H_{light} describes the interaction between the quantum subsystem and the applied laser fields. The Frenkel exciton Hamiltonian will be used to describe the electronic excitations in the quantum system

$$H_{\mathrm{Q}}(t) = hc\left(\sum_i \omega_{0i} B_i^{\dagger} B_i + \sum_{i\neq j} J_{ij} B_i^{\dagger} B_j\right) \tag{2}$$

Here, $B_i^{\dagger}$ and B_i are the bosonic creation and annihilation operators, respectively, for the excitation of site i with central frequency ω_{0i}. J_{ij} denotes the coupling strength between the quantum sites i and j. The formalism presented here can be directly applied to vibrational systems by including a third level on each chromophore (site) and an anharmonicity term.[3] Note that the Frenkel exciton Hamiltonian allows for population transfer within excitation manifolds, but neglects relaxation between them. The interaction of the applied laser field $E(t)$ with the quantum sites, which have transition dipoles μ_i, is given by

$$H_{\mathrm{light}} = hc \sum_i \vec{\mu}_i \cdot \vec{E}(t)(B_i^{\dagger} + B_i) \tag{3}$$

For simplicity we assume throughout this paper that all transition dipole vectors are equal, and parallel to the external electric field. Furthermore, we assume that the laser pulses have an infinitely short (delta peak) duration.

The environment surrounding the quantum system is treated in a classical way using the Brownian oscillator model.[43] A classical treatment of the bath is valid when the thermal energy is large compared to the energy difference between the states of the degrees of freedom treated classically, and for an overdamped mode the inverse correlation time needs to be small compared to the thermal energy. If important modes are present with higher frequencies they should be included directly in the quantum system. In this model collective bath coordinates are used to describe local vibrations of the environment molecules. A single Brownian oscillator with mass M_i and coordinate x_i is coupled to quantum site i to describe local fluctuations of the environment. We assume that each environmental mode feels a harmonic potential so that the Hamiltonian for the classical system is given by

$$H_{\mathrm{C}}(t) = \sum_i \frac{1}{2} k_i x_i^2(t) + \sum_i \frac{1}{2} M_i \dot{x}_i^2(t) \tag{4}$$

where the summations are over all Brownian oscillators. Anharmonic terms can be included without significant additional computational cost. We do not include anharmonic terms within this paper, however, because we will compare the calculated spectra with the HEOM method, which is limited to harmonic modes (Gaussian motion).

The vibrations of the environment molecules influence the quantum system and, vice versa, the potential of the

dx.doi.org/10.1021/jp311668r | J. Phys. Chem. A 2013, 117, 5970−5980

environment depends on the state of the quantum system. The coupling strength J_{ij} and the transition dipole moments μ_i are assumed to be independent of the environment, and will be treated as constants. The quantum-classical interaction Hamiltonian is defined as

$$H_{Q-C}(t) = \sum_i hcD_i x_i(t) B_i^\dagger B_i \tag{5}$$

where D_i denotes the strength of the coupling. From eq 5 it follows that the frequency of the quantum excitations ω_i depends linearly on the classical coordinate coupled to the excitation

$$\omega_i = \omega_{i0} + D_i x_i \tag{6}$$

This is not a fundamental limitation of the Ehrenfest theory but a limitation of the HEOM. A nonlinear classical coordinate dependence will be straightforward to implement. The Brownian oscillators are coupled to a stochastic heat bath with temperature T, and the strength of the coupling is determined by the friction constant γ. The quantum system, classical system, the heat bath, and all the interactions are schematically shown in Figure 1.

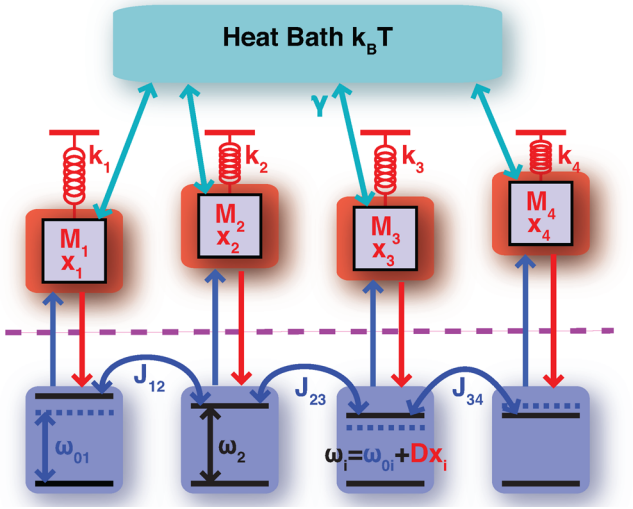

Figure 1. Schematic illustration of the model system. Each quantum site i (blue boxes) is coupled to a single Brownian oscillator (red boxes) with mass M_i and coordinate x_i which is driven by a heat bath with temperature T. The transition energies at the quantum sites are linearly dependent on the classical coordinates.

The time evolution of the quantum system is described by the time-dependent Schrödinger equation

$$i\hbar \frac{d\Phi(t)}{dt} = (H_Q + H_{Q-C}(t))\,\Phi(t) \tag{7}$$

where $\Phi(t)$ is the wave function describing the quantum state. The equation of motion for the Brownian oscillator i in contact with the heat bath is given by the Langevin equation

$$\begin{aligned} M_i\ddot{x}_i(t) &= -k_i x_i(t) - \frac{d}{dx_i}\langle\Phi|H_{Q-C}|\Phi\rangle - \gamma M_i\dot{x}_i(t) + F_{fluc}(t) \\ &= -k_i x_i(t) - hcD_i c_i^*(t)c_i(t) - \gamma M_i\dot{x}_i(t) + F_{fluc}(t) \end{aligned} \tag{8}$$

Here the first term follows from the classical system Hamiltonian. The second term describes the force of the quantum system on the Brownian oscillator, which follows from eq 5 using the mean field approximation[44,45] (Ehrenfest method), and linearly depends on the probability that the quantum site i is excited ($c_i^*(t)c_i(t)$). F_{fluc} describes the effect of the heat bath on the Brownian oscillator and is a Gaussian stochastic random fluctuating force which is related to the friction constant and temperature in the following way:[43]

$$\langle F_{fluc}(t)F_{fluc}(0)\rangle = \begin{cases} \dfrac{2M\gamma k_B T}{\Delta t} & \text{for } t = 0 \\ 0 \quad \text{for } t \neq 0 \end{cases} \tag{9}$$

Here Δt denotes the time interval used for the numerical integration of eq 8.

The time-dependent Schrödinger equation (eq 7) and the equation of motion for the classical system (eq 8) form a set of coupled equations. The time-dependent Schrödinger equation cannot be solved directly for the time-dependent Hamiltonian in eq 7. We therefore assume that the Hamiltonian $H_{Q-C}(t)$ is constant during a short time interval Δt, so that the time evolution operator during this time interval is given by the solution of the time-independent Schrödinger equation

$$\mathbf{U}(t + \Delta t, t) = e^{-(i/\hbar)(H_Q + H_{Q-C}(t))\Delta t} \tag{10}$$

The new quantum state of the system $\Phi(t + \Delta t)$ can then be obtained by multiplying the wave function $\Phi(t)$ with the time evolution operator. The new coordinates of the Brownian oscillator $x_i(t + \Delta t)$ and $\dot{x}_i(t + \Delta t)$ are calculated by numerical integration with a modified Verlet method of eq 8

$$\begin{aligned} \dot{x}_i\left(t + \frac{\Delta t}{2}\right) &= \dot{x}_i(t) + \frac{1}{2}\ddot{x}_i(t)\Delta t \\ x_i(t + \Delta t) &= x_i(t) + \dot{x}_i\left(t + \frac{\Delta t}{2}\right)\Delta t \\ \ddot{x}_i(t + \Delta t) &= -\frac{k_i}{M_i}x_i(t + \Delta t) - hcD_i c_i^*(t)c_i(t) \\ &\quad - \gamma\dot{x}_i\left(t + \frac{\Delta t}{2}\right) + \frac{F_{fluc}(t)}{M_i} \\ \dot{x}_i(t + \Delta t) &= \dot{x}_i\left(t + \frac{\Delta t}{2}\right) + \frac{1}{2}\ddot{x}_i(t + \Delta t)\Delta t \end{aligned} \tag{11}$$

From the new coordinates the Hamiltonian $H_{Q-C}(t + \Delta t)$ is known and the propagation for the next time step is performed resulting in an iterative procedure. The time evolution operator for longer time differences $\mathbf{U}(\tau_i, \tau_j)$ is thus obtained by the time ordered products of the time evolution operators for short intervals Δt. This is identical to the way this is solved in the NISE method.[4,19] In the NISE method the propagation of the classical system however does not depend on the state of the quantum system, and can therefore be done prior to propagating the quantum system. The coupled propagation of the quantum and classical systems is schematically depicted in Figure 2. When the coupling to the heat bath is switched off ($\gamma = 0$), the total energy of the system (quantum plus classical) for calculations including the feedback using this scheme is conserved. For the parameters used in Table 2 (with $\gamma = 0$), however, the energy increases by 1.2% after a trajectory of 100 ps. This is due to the accumulation of numerical errors during the numerical integration where a finite time step is used. All spectral calculations required less than 10 ps of continuous

dx.doi.org/10.1021/jp311668r | J. Phys. Chem. A 2013, 117, 5970−5980

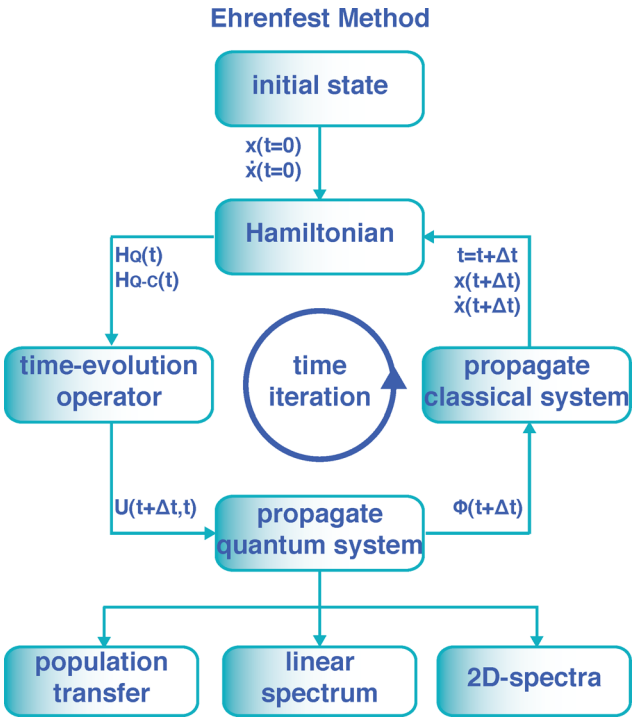

Figure 2. Schematic diagram for the propagation of the state of the quantum system and coordinates of the classical system (Ehrenfest method) from which the population transfer, linear spectrum, and 2D-spectra can be calculated. Each calculation starts with initial conditions for the classical coordinates $x(t = 0)$, $\dot{x}(t = 0)$, which are extracted from a trajectory, in which the quantum system is in the ground state, separated by multiple correlation times.

propagation, implying that this numerical error does not affect the spectra presented here. The scheme in Figure 2 shows that the population transfer, linear spectrum, and two-dimensional spectra can be calculated as will be explained below.

The population transfer between an initial eigenstate i and a final eigenstate f is calculated by

$$P_{fi}(t) = \langle |\langle \Phi_f(t)|\mathbf{U}(t, 0)|\Phi_i(0)\rangle|^2 \rangle_E \quad (12)$$

Here $\langle ... \rangle_E$ denotes the ensemble average, which is calculated by summing results from $N_{samples}$ different initial starting points for the classical system which are extracted from a trajectory during which the quantum-system is in the ground state (no feedback) separated by 100 ps. The inner brackets denote the usual Dirac notation from quantum mechanics.

For the linear absorption spectrum the system is excited by interacting with a laser pulse at a time τ_1, after which a signal is emitted by the system at a time τ_2. The absorption spectrum is calculated by taking the imaginary part of the Fourier transform, over the time between the laser pulse and the signal $t_1 = \tau_2 - \tau_1$, of the two-point correlation function of the transition dipoles

$$S_A(\omega) = \mathrm{Im}\left[\int_0^\infty \frac{i}{\hbar}\langle \mu^{01}(\tau_2)\mathbf{U}^{11}(\tau_2, \tau_1)\mu^{10}(\tau_1)\rangle_E e^{-i\omega t_1}\, dt_1\right] \quad (13)$$

Here μ^{10} denotes the transition dipole moment between the initial ground state (denoted 0) and the final excited state (denoted 1). The superscript in the propagator (11) denotes the propagation when there is a single excitation in the quantum system (single excited state). A lifetime T_1 of the excited state can be included in an ad hoc way by multiplying the response function by

$$\Gamma_{LA} = e^{-t_1/2T_1} \quad (14)$$

Our main focus is to simulate two-dimensional electronic spectra described by the third-order response function. In this experiment, three laser pulses are applied at times τ_1, τ_2, and τ_3 and the signal is measured at a time τ_4.[1,2,4,43] Using impulsive pulses and applying the Rotating Wave Approximation[1] the signal for the third-order response function has six contributions. These can be represented by the double-sided Feynmann

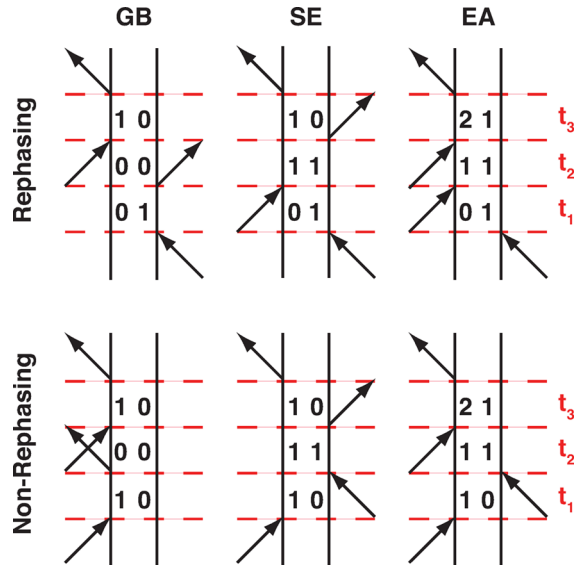

Figure 3. Double-sided Feynmann diagrams that contribute to the third-order response. Three laser fields are applied with time delays $t_1 = \tau_2 - \tau_1$ and $t_2 = \tau_3 - \tau_2$. The signal is emitted by the system a time $t_3 = \tau_4 - \tau_3$ after the third laser pulse. The numbers 0, 1, and 2 denote the ground state, single excited states, and double excited states, respectively.

diagrams depicted in Figure 3.[43] The six contributions are the rephasing and nonrephasing parts of the ground state bleach (GB), the stimulated emission (SE) and the excited state absorption (EA). The first laser pulse brings the quantum system in a coherence between a single excited state and the ground state (01 (rephasing) or 10 (nonrephasing)) for all diagrams. For the GB-diagram the interaction with the second laser pulse brings the system back in the ground state. The interaction with the third laser pulse brings the system in a coherence between the single excited state and the ground state (10). At a time τ_4 the system relaxes back to the ground state by emitting the signal. The SE-diagram differs from the GB-diagram only during the waiting time t_2, where the system is in a single excited state or a coherence between two single-excited states instead of the ground state. The excited state absorption diagrams are the same as the stimulated emission diagrams until the third laser pulse. The third laser pulse brings the system in a coherence between a double excited state (a state where two sites are excited) and a single excited state (21). The responses of all six diagrams can be obtained by calculating the following ensemble averages

dx.doi.org/10.1021/jp311668r | J. Phys. Chem. A 2013, 117, 5970−5980

$$S^{R}_{GB}(t_1, t_2, t_3) = -\left(\frac{i}{\hbar}\right)^3 \langle\langle 0|\mu^{01}(\tau_1)\mathbf{U}^{11}(\tau_1, \tau_2)\mu^{10}(\tau_2)\mu^{01}(\tau_4)\mathbf{U}^{11}(\tau_4, \tau_3)\mu^{10}(\tau_3)|0\rangle\rangle_E$$

$$S^{R}_{SE}(t_1, t_2, t_3) = -\left(\frac{i}{\hbar}\right)^3 \langle\langle 0|\mu^{01}(\tau_1)\mathbf{U}^{11}(\tau_1, \tau_3)\mu^{10}(\tau_3)\mu^{01}(\tau_4)\mathbf{U}^{11}(\tau_4, \tau_2)\mu^{10}(\tau_2)|0\rangle\rangle_E$$

$$S^{R}_{EA}(t_1, t_2, t_3) = \left(\frac{i}{\hbar}\right)^3 \langle\langle 0|\mu^{01}(\tau_1)\mathbf{U}^{11}(\tau_1, \tau_4)\mu^{12}(\tau_4)\mathbf{U}^{22}(\tau_4, \tau_3)\mu^{21}(\tau_3)\mathbf{U}^{11}(\tau_3, \tau_2)\mu^{10}(\tau_2)|0\rangle\rangle_E$$

$$S^{NR}_{GB}(t_1, t_2, t_3) = -\left(\frac{i}{\hbar}\right)^3 \langle\langle 0|\mu^{01}(\tau_4)\mathbf{U}^{11}(\tau_4, \tau_3)\mu^{10}(\tau_3)\mu^{01}(\tau_2)\mathbf{U}^{11}(\tau_2, \tau_1)\mu^{10}(\tau_1)|0\rangle\rangle_E$$

$$S^{NR}_{SE}(t_1, t_2, t_3) = -\left(\frac{i}{\hbar}\right)^3 \langle\langle 0|\mu^{01}(\tau_2)\mathbf{U}^{11}(\tau_2, \tau_3)\mu^{10}(\tau_3)\mu^{01}(\tau_4)\mathbf{U}^{11}(\tau_4, \tau_1)\mu^{10}(\tau_1)|0\rangle\rangle_E$$

$$S^{NR}_{EA}(t_1, t_2, t_3) = \left(\frac{i}{\hbar}\right)^3 \langle\langle 0|\mu^{01}(\tau_2)\mathbf{U}^{11}(\tau_2, \tau_4)\mu^{12}(\tau_4)\mathbf{U}^{22}(\tau_4, \tau_3)\mu^{21}(\tau_3)\mathbf{U}^{11}(\tau_3, \tau_1)\mu^{10}(\tau_1)|0\rangle\rangle_E \quad (15)$$

Here the time evolution operators have superscript indices denoting the propagation of a single excited state (11) or a double excited state (22). The propagator of the ground state is given by unity and is omitted in the expressions above. The coupled time evolution of the quantum and classical systems is calculated following the scheme depicted in Figure 2. The force on the Brownian oscillator i depends on the probability that the quantum site i is excited (eq 8). When the system is in a coherence between two states, the feedback of the quantum system on the classical system is taken into account separately for the ket- and bra-side which are described by different wave functions $\Phi^{K}(t)$ and $\Phi^{B}(t)$ respectively. The Langevin equation for the Brownian oscillator i then reads

$$M_i\ddot{x}_i(t) = -kx_i(t) - \frac{hcD_i}{2}(c^*_{Ki}(t)c_{Ki}(t) + c^*_{Bi}(t)c_{Bi}(t)) - \gamma M_i\dot{x}_i(t) + F_{fluc}(t) \quad (16)$$

thus assuming a mean classical path approximation for coherences. In the absence of relaxation between the excitation manifolds in the present Hamiltonian, the lifetime T_1 of the excited states can be taken in to account in an ad hoc way by multiplying the response functions in eq 15 by the following factor

$$\Gamma(t_3, t_2, t_1) = e^{-(t_1+2t_2+t_3)/2T_1} \quad (17)$$

The signals in the frequency domain (for a fixed waiting time t_2) resulting from the rephasing and nonrephasing diagrams are obtained by Fourier transforming over the times t_1 and t_3

$$S^{R}(\omega_1, t_2, \omega_3) = \int_0^{t_1^{max}}\int_0^{t_3^{max}} (S^{R}_{GB}(t_1, t_2, t_3) + S^{R}_{SE}(t_1, t_2, t_3) + S^{R}_{EA}(t_1, t_2, t_3))e^{-i(\omega_1 t_1 - \omega_3 t_3)}\, dt_1\, dt_3$$

$$S^{NR}(\omega_1, t_2, \omega_3) = \int_0^{t_1^{max}}\int_0^{t_3^{max}} (S^{NR}_{GB}(t_1, t_2, t_3) + S^{NR}_{SE}(t_1, t_2, t_3) + S^{NR}_{EA}(t_1, t_2, t_3))e^{-i(\omega_1 t_1 - \omega_3 t_3)}\, dt_1\, dt_3 \quad (18)$$

In general the response function should be integrated over times t_1 and t_3 from zero to infinity. The response function, however, vanishes at finite t_1 and t_3 times, either due to dephasing or the finite lifetime of the excitation, and therefore, in practice finite times t_1^{max} and t_3^{max} can be used. The absorptive spectrum is obtained by adding the imaginary parts of the responses resulting from the rephasing and nonrephasing diagrams.[46] All two-dimensional spectra presented in this paper are these absorptive spectra.

Hierarchical Equations of Motion. The HEOM implementation is an exact method to calculate the dynamics of an open quantum system and observables such as the two-dimensional spectrum.[47] A derivation and extensive explanation of the method can be found in refs 35, 47, and 48. Here we only give a brief explanation of the method and an overview of the approximations we make.

The Hamiltonian we use for the HEOM is very similar to eq 1.[48] The quantum system consisting of coupled chromophores is again described by the Frenkel exciton Hamiltonian. A single Brownian oscillator (phonon mode) is coupled to each chromophore which in contrary to the previous section is described quantum mechanically as well. The time evolution of the density matrix in the HEOM approach is described by a set of infinitely many coupled differential equations. The first of these differential equations describes the time evolution of the reduced density operator $\sigma^{(0,0)}(t)$ which is the trace of the total density matrix over all environmental degrees of freedom. The reduced density operator contains all the information of the quantum system. The number of superscript indices is equal to the number of chromophores in the quantum system so that in this case we treat a dimer. The time evolution of the reduced density operator depends on auxiliary operators, for which one or all of these indices are larger than zero, which account for the state of the environment as well as correlations between the system and the environment. The reduced density operator only couples to auxiliary operators for which one of the indices

dx.doi.org/10.1021/jp311668r | J. Phys. Chem. A 2013, 117, 5970−5980

is increased by one ($\sigma^{(1,0)}(t)$ and $\sigma^{(0,1)}(t)$). The time evolution of these auxiliary operators is again described by a differential equation which depends on other operators for which one of the indices can is either increased or lowered by one, but cannot become negative. The time evolution of these higher order auxiliary operators are again described by a differential equation which has a very similar form and depends on higher order auxiliary operators (the hierarchy).[47]

The HEOM approach is exact if infinitely many auxiliary operators are taken into account. In practice however the number of auxiliary operators is truncated by defining a depth of the hierarchy N_{depth}. The auxiliary operators for which the sum of the indices is larger than the depth are not included. We use a fourth order Runga-Kutta method to numerically integrate the set of differential equations and calculate the (two-dimensional) spectra.[35] When the quantum system is in the ground state there is no coupling between the chromophores and environment. The equilibrium state for the phonon modes in this case is when all auxiliary operators are equal to zero. When the system is excited at $t = 0$ by a laser pulse this is no longer the equilibrium state due to the coupling between the quantum system and the environment. It is assumed that the laser pulse only excites the quantum system and does not interact with the phonon modes. After the quantum system is excited there will be an exchange of energy with the environment until the new equilibrium state is reached, eventually resulting in nonzero constant values of the auxiliary operators.

We assume that the spectral density, which quantifies the coupling to the phonon modes and their spectral density, is of Debye type. This corresponds to the overdamped Brownian oscillator model with a harmonic potential. We do not include the Matsubara frequencies; this results in a high temperature approximation and is valid when $k/(M\gamma k_B T c) \ll 1$.

RESULTS AND DISCUSSION

Stokes Shift for a Single Two-Level Quantum Site. In this subsection we consider a single two-level quantum site which is coupled to a single Brownian oscillator that is driven by a heat bath. When the quantum site is in the ground state the minimum of the potential of the Brownian oscillator is located at $x_0 = 0$. When the quantum site is in the excited state the minimum of the potential is shifted to $x_0 = -(hcD/k)$ due to the feedback of the quantum site. This subsequently leads to a shift in the central frequency, the so-called Stokes shift, of the quantum site

$$\Delta\omega_{\text{stokes}} = \Delta x_0 D = -\frac{hcD^2}{k} \tag{19}$$

It takes time however before the position of the Brownian oscillator is adjusted to the new potential. In the strongly overdamped limit $\gamma \gg 2(k/M)^{1/2}$ the correlation function for the coordinate of the Brownian oscillator is given by[43]

$$\langle x(t)x(0)\rangle = \frac{k_B T}{k} e^{-t/t_c} \tag{20}$$

where $t_c = (M\gamma)/k$ is the correlation time. The prefactor $(k_B T/k)^{1/2}$ determines the amplitude of the oscillations of the Brownian oscillator. The factor is directly related to the width of the peaks in the spectra resulting from the quantum site, because of the linear dependence of the transition energy on the position of the Brownian oscillator. In the overdamped limit the Brownian oscillator model thus reduces to two parameters, the correlation time t_c and the size of the fluctuations of the transition frequency $\lambda = D(k_B T/k)^{1/2}$.

In Figure 4 the simulated two-dimensional spectra are shown for the single quantum site using the NISE, Ehrenfest, and HEOM methods for waiting times $t_2 = 0$ ps and $t_2 = 5$. The used parameters are given in Table 1. We tested that the employed time step given in the table was sufficiently small to eliminate observable numerical errors due to the propagation method. The spectra are the sum of the groundstate bleach and stimulated emission diagrams in Figure 3. The excited state absorption diagrams do not contribute to these spectra, since we are considering a single two-level quantum site. When the waiting time is 0, the spectra for the three calculations are essentially identical, showing a diagonally elongated peak with central position at $\omega_3 = \omega_0 = 12000$ cm^{-1}. The peak is

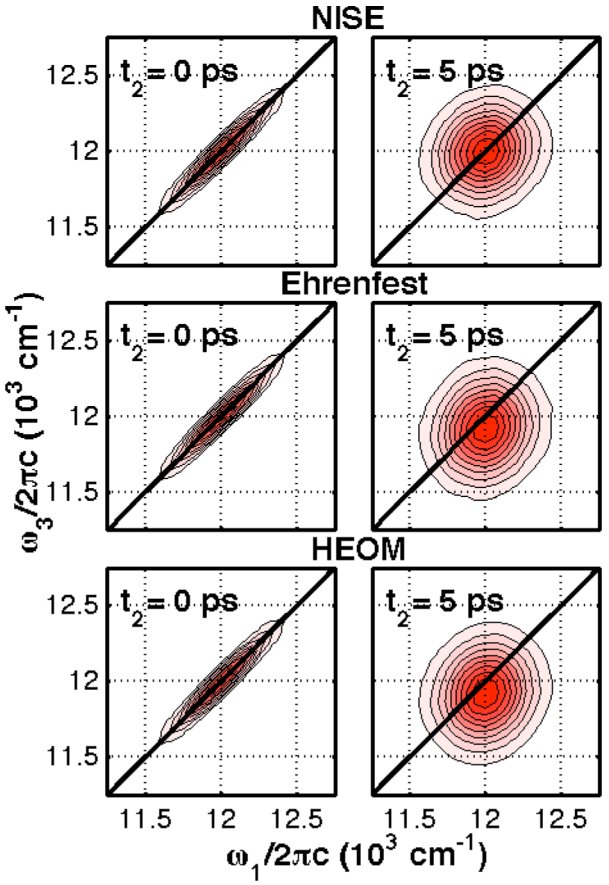

Figure 4. Simulated two-dimensional spectra for a single quantum-site for $t_2 = 0$ ps and $t_2 = 5$ ps using the NISE, Ehrenfest and HEOM methods (top to bottom). The contour levels are plotted at every 10% of the maximum absolute peak value in the spectra. The red color indicates negative valued peaks and the white color denotes zero intensity.

Table 1. The Parameters for the Single Quantum Site Simulations

Δt (ps)	0.001	T (K)	300	λ (cm^{-1})	195
$t_1^{\max}$ (ps)	0.5	N_{samples}	50000	t_c (ps)	2.5
$t_3^{\max}$ (ps)	0.5	ω_0 (cm^{-1})	12000	N_{depth}	80
T_1 (ps)	1	γ (ps^{-1})	50		

dx.doi.org/10.1021/jp311668r | J. Phys. Chem. A 2013, 117, 5970−5980

diagonally elongated because the dephasing time of the response function ($(\lambda c)^{-1}$ = 0.17 ps) and the waiting time both are short compared to the correlation time (t_c = 2.5 ps) of the Brownian oscillator. Therefore there is no time for the Brownian oscillator to change coordinate, so that the pump and probe frequency are equal. For the same reason the NISE method, which does not include the feedback, gives the same result as the Ehrenfest method, since there is no time for the Brownian oscillator to adjust to the new potential. When t_2 = 5 ps, elliptical peaks are obtained for all three calculations due to spectral diffusion, caused by the fact that the fluctuations in the oscillator's displacement cause fluctuations in the transition frequency of the quantum site. When there is no feedback, the central peak position along ω_3 is still ω_3 = 12000 cm^{-1}, because the average coordinate of the Brownian oscillator remains x_0 = 0. But for the calculations including the feedback (Ehrenfest and HEOM) the central peak position along ω_3 is shifted to a lower value due to the Stokes shift, since there is enough time for the Brownian oscillator to adjust to the shift in the potential. Energy has transferred from the quantum system to the environment. The Ehrenfest and HEOM methods show identical behavior.

During the waiting time the quantum system is in the groundstate for the groundstate bleach diagrams and in the excited state for the stimulated emission diagrams. Consequently only the stimulated emission diagrams include the Stokes shift during the waiting time for the calculations including the feedback. The total spectra for t_2 = 5 ps show a single peak which is the sum of a GB contribution with central peak position along ω_3 at the central frequency ω_0 and a SE contribution with a central peak position located at a lower probe frequency due to the Stokes shift. Only a single peak is observed since the linewidths of the two contributions are larger than the Stokes shift. In Figure 5 the central peak position along ω_3 for the SE diagrams as a function of the waiting time is shown for the three calculations. If there is no feedback the frequency stays approximately constant around the central frequency of the quantum site. For the calculations including the feedback the central frequency decreases as the waiting time is increased until the new equilibrium is reached. According to eq 19, it is expected for the parameters used that the frequency is shifted by $\Delta\omega_{stokes}$ = 183 cm^{-1}, which corresponds nicely with shifts observed for the Ehrenfest and HEOM methods. The exponential fit for the peak position as a function of the waiting time for the Ehrenfest method (black dashed line) gives a relaxation constant τ_{Stokes} = 2.6 ps, which is essentially equal to the correlation time of the bath (t_c = 2.5 ps), as is expected.

The present method relies on (nonequilibrium) trajectories to calculate the response and not on the correlation function. The Stokes shift here thus arises from the inclusion of the feedback force, where correlation function based methods usually account for this physical phenomena through the imaginary part of the quantum correlation function.[43]

Two-Dimensional Spectra for a Coupled Dimer. In this subsection we consider two coupled quantum sites with different central excitation frequencies and compare the two-dimensional spectra obtained using the three different methods. We assume that the parameters describing the Brownian oscillators and coupling to the heat bath are equal for both quantum sites. We use the parameters given in Table 2. We verified that the employed time step given in the table was sufficiently small to eliminate observable numerical errors due to the propagation method. In Figure 6 the linear absorption spectra are shown for calculations using the NISE, Ehrenfest, and HEOM methods. The linear spectra obtained essentially

Table 2. Parameters Used for Simulations of the Dimer Coupled to the Classical System and Heat Bath

Δt (ps)	0.005	$N_{samples}$	60000	λ (cm^{-1})	198
t_1^{max} (ps)	0.5	ω_{01} (cm^{-1})	11500	t_c (ps)	0.22
t_3^{max} (ps)	0.5	ω_{02} (cm^{-1})	12000	N_{depth}	20
T_1 (ps)	1	J (cm^{-1})	100		
T (K)	300	γ (ps^{-1})	50		

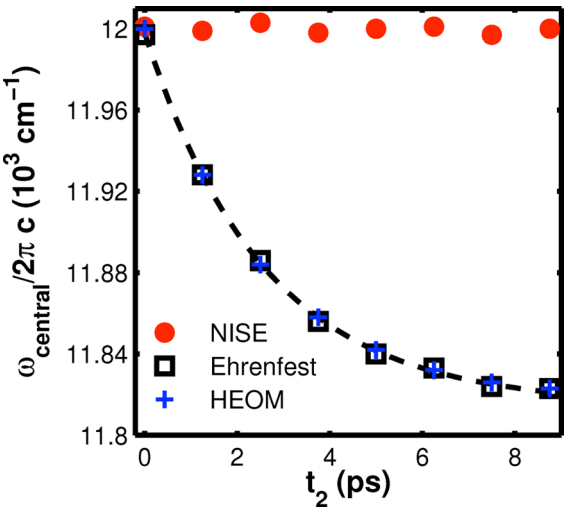

Figure 5. Central peak position along the ω_3 axis of the two-dimensional spectra resulting from the stimulated emission diagrams for the single quantum site as a function of the waiting time t_2, for spectra calculated using the NISE (red circle), Ehrenfest (square) and HEOM methods (blue cross). The solid blue line is the result of an exponential fit $\bar{\omega}_3(t) = \bar{\omega}_3(\infty) + \Delta_{stokes}e^{-t/\tau_{stokes}}$.

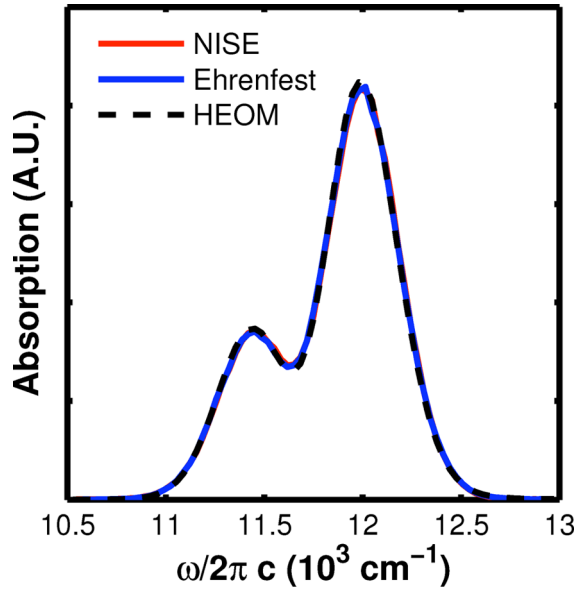

Figure 6. Linear spectrum for the coupled dimer calculated using the NISE (red line), Ehrenfest (blue line), and HEOM (black dashed line) methods.

dx.doi.org/10.1021/jp311668r | J. Phys. Chem. A 2013, 117, 5970−5980

show no difference. This results from the fact that the dephasing time is shorter than the correlation time of the environment, so that the difference in dynamics of the environment has no time to affect the spectrum.

In Figure 7 the two-dimensional spectra for the coupled dimer are shown for the three different methods for waiting

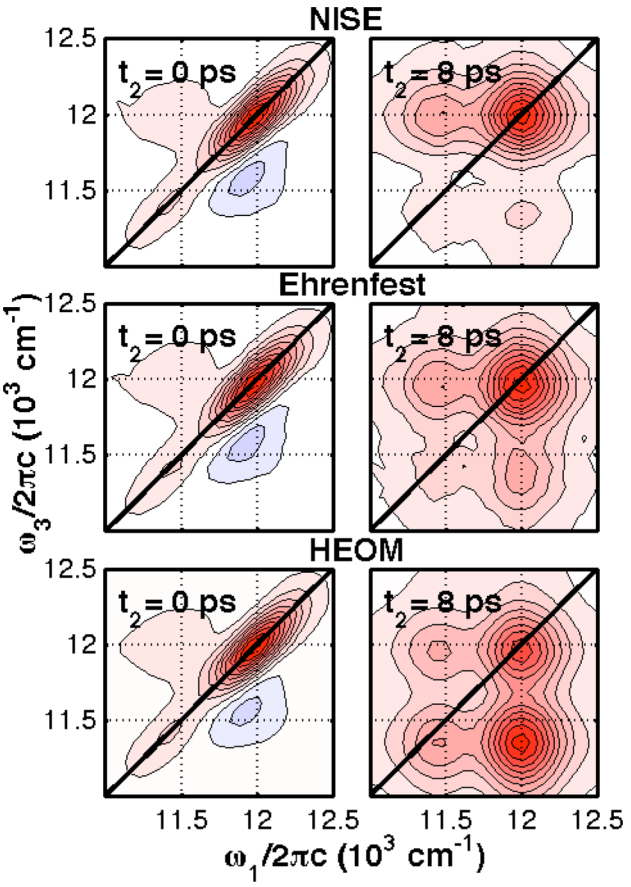

Figure 7. Simulated two-dimensional spectra using the NISE, Ehrenfest, and HEOM methods for the coupled dimer for waiting times t_2 = 0 ps and t_2 = 8 ps. The red colors indicate negative valued peaks and the blue colors indicate positive valued peaks. The contour levels are plotted at intervals of 10% of the absolute maximum of the spectrum starting at 95%.

times t_2 = 0 ps and t_2 = 8 ps. For the parameters chosen the correlation time of the environment is short compared to the population transfer time. In this way we can distinguish between effects in the spectra resulting directly from dynamics of the environment (such as spectral diffusion and the Stokes shift) which happen on a short time scale and the population transfer taking place at longer times. When the waiting time is 0 ps all three calculated spectra are identical. There is a positive cross peak (blue color) which results from the excited state absorption diagrams. When the waiting time is 8 ps the lineshapes are broader due to spectral diffusion. There are clear differences in the spectra for the three methods. Especially the cross-peaks show different intensities when the waiting time is increased. In Figure 8 the intensities of the upper (ω_1 = 11488 cm^{-1}) and lower (ω_1 = 12012 cm^{-1}) cross peaks are shown as a function of the waiting time for the three methods. The growth of the lower cross peak is smallest for the NISE method and largest for the HEOM method. The Ehrenfest approach is somewhere in between these two. The opposite behavior is

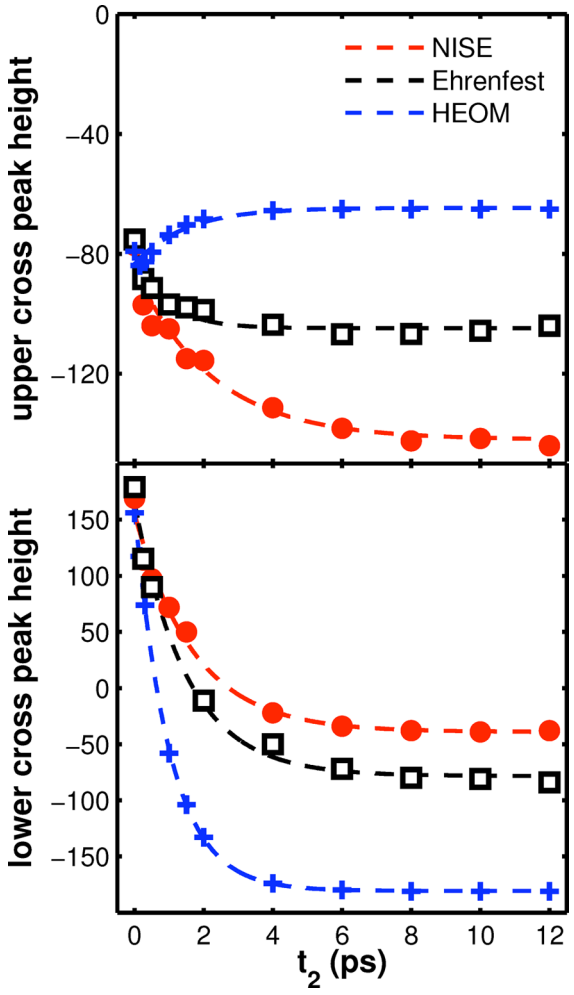

Figure 8. Peak height of the upper cross peak located at $\omega_1 \approx$ 11488 cm^{-1} (upper graph) and lower cross peak located at $\omega_1 \approx$ 12012 cm^{-1} (lower graph) as a function of the waiting time for the NISE (red circle), Ehrenfest (square), and HEOM (cross) methods. The boxes represent data points taken from the calculated two-dimensional spectra and the dashed lines are results of exponential fits ($I(t) = I_0(\infty) + \Delta_{grow}e^{-\Gamma_d t}$).

observed for the upper cross peak. The growth of the lower cross peak is determined by the population transfer from the high energy eigenstate (which is initially excited by the pump pulse) and the low energy eigenstate.

For the HEOM method it is not possible to calculate the population transfer between the instantaneous eigenstates because the site energies as a function of time are not explicitly known. This is because the HEOM is an ensemble average method and thus does not allow the extraction of information of the Hamiltonian of individual trajectories from the reduced density matrix at all times. In Figure 9 the population transfer between the instantaneous eigenstates is plotted as a function of time for the NISE and Ehrenfest methods. There is more population transfer from the high to the low energy eigenstate for the Ehrenfest method than for the NISE method. When the high energy eigenstate is excited by the pump pulse, the Stokes shift will lower the energy and the energy difference between the eigenstates is decreased. This increases the population transfer from the high energy eigenstate to the low energy eigenstate resulting in a larger growth of the lower cross-peak, as is observed. For the upper cross peak the exact opposite is

dx.doi.org/10.1021/jp311668r | J. Phys. Chem. A 2013, 117, 5970−5980

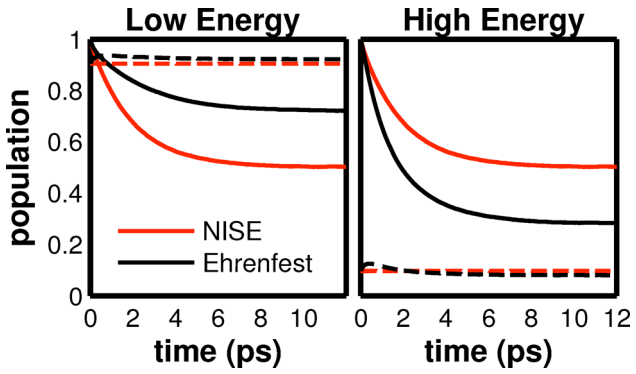

Figure 9. Ensemble average of the populations of the instantaneous eigenstates as a function of time for a coupled dimer using the NISE (red) and Ehrenfest (blue) methods. In the left graph the low energy eigenstate is initially excited and in the right one the high energy eigenstate. The dashed lines denote the expected equilibrium populations of the instantaneous eigenstates if a Boltzmann distribution within the quantum system is obeyed. These lines differ for the two methods because of the Stokes shift, which is only included in the Ehrenfest method.

observed since the Stokes shift increases the energy difference between the eigenstates, resulting in less population transfer. The NISE method is a high temperature approximation and the probability in equilibrium for a state to be excited is independent of the energy of the state and, therefore, is equal for each state.[4] This is only valid when the thermal energy is large compared to the energy difference between the states which is not the case for the parameters chosen. For the Ehrenfest method it is more likely to end up in the low energy eigenstate than in the high energy eigenstate when the energy difference is larger than or comparable to the thermal energy in contrary to the NISE method. Owing to the mean field approach, the Ehrenfest method does not result in a Boltzmann distribution in the quantum system, as previously discussed in detail by Tully et al.[42] This explains the difference with the HEOM result, which shows an even larger growth of the lower cross peak. Although the Ehrenfest method does not reproduce the exact result, an improved behavior is observed compared to the NISE method.

Since the correlation time of the bath is short, the growth of the cross peaks after several correlation times solely depends on the population transfer. The decay time Γ_d of the cross peak height should, therefore, be identical to the decay rate of the population transfer in Figure 9. The results for an exponential fit of the cross peak height and population transfer are summarized in Table 3. From this Table it is clear that the fit parameters for the population transfer from the low energy eigenstate to the high energy one of Figure 9 and the corresponding growth of the upper cross peak in Figure 8 do not coincide. The changes in peak height happen on a short time scale where spectral diffusion still takes place. Therefore the parameters do not match very well. For the lower cross peak, where the changes in peak height occur at longer waiting times, the fit parameters coincide with the parameters obtained for the population transfer from the high energy eigenstate to low energy one.

Table 3. Results of the Exponential Fits $I(t) = I_0(\infty) + I_0 e^{-\Gamma_d t}$ of the Curves in Figures 9 and 8 for the Upper and Lower Cross Peaks

	cross peak Γ_d (ps^{-1})	pop trans. Γ_d (ps^{-1})
NISE upper	0.45	0.52
Ehrenfest upper	1.14	0.40
NISE lower	0.59	0.56
Ehrenfest lower	0.67	0.62

The energy difference chosen here is quite large compared to the thermal energy so that we could study the cross peak growth independently of the diagonal peaks. The Ehrenfest method will give results closer to the HEOM method when the energy difference is smaller. In the extreme situation where the sites have the same transition energies, the NISE and Ehrenfest methods both result in a Boltzmann distribution. When there is a Stokes shift, the energy difference between the eigenstates will increase however. This will decrease the population transfer if the Stokes shift is large compared to the coupling, an effect that influences the shape of the two-dimensional spectra. Such a trapping effect is included in the Ehrenfest and HEOM methods, but is neglected in the NISE method.

In general the correlation time of the environment is not necessary small compared to the transfer time. In this case the transfer time cannot be obtained simply by measuring the height of the cross peaks. Simulations are therefore needed for interpreting the experimental spectra. Furthermore, in real systems the correlation functions may not be in the overdamped limit and the population transfer may show coherent oscillations resulting in very complex spectra. Such effects can be included in the Ehrenfest method. Here we have chosen harmonic potentials resulting in Gaussian dynamics to be able to compare the Ehrenfest method with the exact result provided by HEOM. When different forms for the potentials are used, the signature of the environment can become much more pronounced.[30] For such potentials HEOM is no longer exact.

Thermalization. From Figure 9, the probability for finding the coupled dimer in the low energy eigenstate in equilibrium (long waiting time) for the Ehrenfest method is $P_L = 0.72$. If a Boltzmann distribution is obeyed the probability to occupy the low energy instantaneous eigenstate in equilibrium for the parameters used is $P_L = 0.9$. For the Ehrenfest method the quantum system solely does not obey a Boltzmann distribution. When the Brownian oscillators are not coupled to the heat bath the energy within the quantum plus classical system is conserved which is clear from the Hamiltonian in eq 1. Therefore, when there is a coupling to the heat bath the total quantum classical system is expected to give a Boltzmann distribution of energy. When a Boltzmann distribution is obeyed the probability for the system to have a certain energy is given by

$$D(T, E) = \frac{g(E)e^{-\beta E}}{Z(T)} \tag{21}$$

where $g(E)$ denotes the degeneracy, that is, the number of available states of that energy, $Z(T)$ denotes the partition function, and $\beta = 1/k_B T$. In the top graph of Figure 10 the probability that the system of section 3.2 has a specific energy is plotted for different temperatures. This figure was created by counting the number of times the quantum-classical system has a specific energy, with the quantum system in a single excited state, over a trajectory of 10^8 time steps. When the temperature is increased, higher energy states become more probable as is expected. The quotient of two distributions of energy for

dx.doi.org/10.1021/jp311668r | J. Phys. Chem. A 2013, 117, 5970−5980

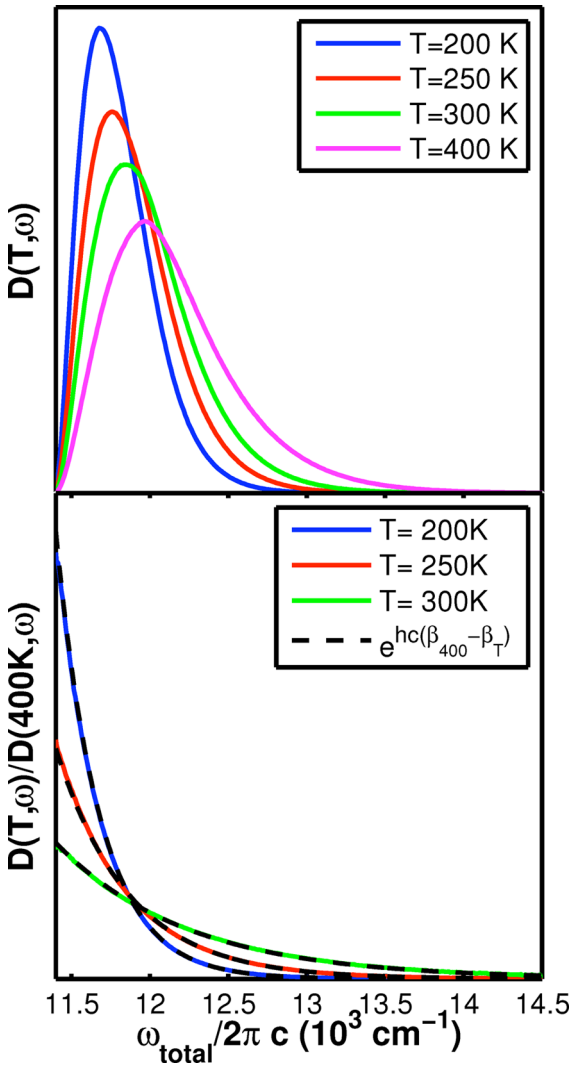

Figure 10. Top: Distribution of the total energy of the quantum-classical system for the coupled dimer of section 3.2 in a single excited state, for temperatures T = 200 K, T = 250 K, T = 300 K, and T = 400 K. Bottom: Quotient of the distributions for T = 200 K, T = 250 K, and T = 300 K in the top graph and the distribution for T = 400 K. The black dashed lines show the same quotients expected if the distributions of energy obey Boltzmann statistics.

different temperatures of a certain system is independent of the degeneracy

$$\frac{D(T_1, E)}{D(T_2, E)} = \frac{Z(T_2)}{Z(T_1)} e^{(\beta_2 - \beta_1)E} \tag{22}$$

In the bottom graph of Figure 10, the quotient between distributions with different temperatures is plotted. The black dashed lines show the results expected if the distributions obey Boltzmann statistics in eq 22. The quotient between distributions for different temperatures match the black dashed lines perfectly. We, thus conclude that when using the Ehrenfest method a Boltzmann distribution within the quantum system is not obtained; however, the total energy of the quantum and classical systems does obey a Boltzmann distribution as is expected.

CONCLUSIONS

In this paper we presented an approach to perform mixed quantum-classical simulations of two-dimensional spectra. We used the Ehrenfest method to include the change in potential the classical system feels when transitions occur in the quantum mechanical system. We studied how this interaction influences the shape of two-dimensional spectra by comparing simulated spectra for calculations that include (Ehrenfest) and neglect (NISE) the feedback of the quantum system. As a benchmark we compared the spectra with the HEOM method.

We showed for a single quantum site that the feedback of the quantum system leads to a Stokes shift when the dephasing-time of the response function is comparable to (or longer than) the correlation time of the classical system. The waiting time dependence of the magnitude of the Stokes shift is identical to the correlation time of the environment. The results obtained with the Ehrenfest method match the HEOM method perfectly in contrast to the NISE method where the Stokes shift is absent.

For two coupled quantum sites that have different central excitation frequencies we showed that the three methods result in identical spectra when the waiting time is zero. The Stokes shift resulting from the feedback of the quantum system influences the population transfer between the eigenstates. When the low energy eigenstate is excited, the Stokes shift increases the energy difference between the eigenstates which decreases the rate of population transfer to the high energy eigenstate. Vice versa, when the high energy eigenstate is initially excited, the energy difference between the eigenstates is reduced by the Stokes shift, and the rate of population transfer is increased. We showed that the difference in the population transfer for the NISE and Ehrenfest methods is directly related to the differences in the growth of the cross peaks of the two-dimensional spectra when the waiting time is increased. The Ehrenfest method results in slightly improved spectra as compared to NISE, but by far does not reproduce the HEOM result. For the parameters chosen the energy difference between the eigenstates is much larger than the thermal energy. The Ehrenfest method does not reproduce a Boltzmann distribution for the quantum system in this case. The Ehrenfest method is expected to give more accurate results when the couplings and energy differences of the site energies are small compared to the thermal energy. We showed that although a Boltzmann distribution within the quantum system is absent for the Ehrenfest method, the distribution of energy of the total quantum-classical system does obey Boltzmann statistics when coupled to a heat bath. In an ongoing study we found that using a surface-hopping approach can be used to improve the cross-peak intensities in the two-dimensional spectra.[49]

In conclusion, including the feedback using the Ehrenfest method is a significant improvement compared to the NISE method, as it allows for a description of the Stokes shift. The presented approach allows one to account for non-Condon and non-Gaussian effects as well as a general classical environment that may be described with a MD simulation as long as the bath degrees of freedom can be considered classical. The computational cost for treating larger systems is expected to be significantly lower for the Ehrenfest method[20] compared to HEOM even though considerable effort has been made developing time efficient and highly parallel HEOM codes.[34,50,51]

dx.doi.org/10.1021/jp311668r | J. Phys. Chem. A 2013, 117, 5970−5980

AUTHOR INFORMATION

Corresponding Author

*E-mail: c.p.n.van.der.vegte@rug.nl; agdijkstra@gmail.com; j.knoester@rug.nl; t.l.c.jansen@rug.nl.

Notes

The authors declare no competing financial interest.

ACKNOWLEDGMENTS

This work is part of the research programme of the Foundation for Fundamental Research on Matter (FOM), which is part of The Netherlands Organization for Scientific Research (NWO). T.L.C.J. acknowledges The Netherlands Organization for Scientific Research (NWO) for support through a VIDI grant.

REFERENCES

(1) Hamm, P.; Zanni, M. T. *Concepts and Methods of 2D Infrared Spectroscopy*; Cambridge University Press: Cambridge, 2011.
(2) Brixner, T.; Stenger, J.; Vaswani, H. M.; Cho, M.; Blankenship, R. E.; Fleming, G. R. *Nature* **2005**, *434*, 625.
(3) Hamm, P.; Lim, M. H.; Hochstrasser, R. M. *J. Phys. Chem. B* **1998**, *102*, 6123.
(4) Jansen, T. L. C.; Knoester, J. *Acc. Chem. Res.* **2009**, *42*, 1405−1411.
(5) McRobbie, P. L.; Hanna, G.; Shi, Q.; Geva, E. *Acc. Chem. Res.* **2009**, *42*, 1299−1309.
(6) Ghosh, A.; Qiu, J.; DeGrado, W. F.; Hochstrasser, R. M. *Proc. Natl. Acad. Sci.* **2011**, *108*, 6115−6120.
(7) Mohammed, O. F.; Pines, D.; Dreyer, J.; Pines, E.; Nibbering, E. T. J. *Science* **2005**, *310*, 83.
(8) Siwick, B. J.; Cox, M. J.; Bakker, H. J. *J. Phys. Chem. B* **2008**, *112*, 378.
(9) Fecko, C. J.; Eaves, J. D.; Loparo, J. J.; Tokmakoff, A.; Geissler, P. L. *Science* **2003**, *301*, 1698.
(10) Asbury, J. B.; Steinel, T.; Fayer, M. D. *J. Phys. Chem. B* **2004**, *108*, 6544−6554 Article..
(11) Backus, E. H. G.; Nguyen, P. H.; Botan, V.; Pfister, R.; Moretto, A.; Crisma, M.; Toniolo, C.; Stock, G.; Hamm, P. *J. Phys. Chem. B* **2008**, *112*, 9091.
(12) Woutersen, S.; Hamm, P. *J. Chem. Phys.* **2001**, *115*, 7737.
(13) Jansen, T. L. C.; Knoester, J. *Biophys. J.* **2008**, *94*, 1818−1825.
(14) King, J. T.; Baiz, C. R.; Kubarych, K. J. *J. Phys. Chem. A* **2010**, *114*, 10590−10604.
(15) Engel, G. S.; Calhoun, T. R.; Read, E. L.; Ahn, T. K.; Mancal, T.; Cheng, Y. C.; Blankenship, R. E.; Fleming, G. R. *Nature* **2007**, *446*, 782.
(16) Scholes, G. D.; Fleming, G. R.; Olaya-Castro, A.; van Grondelle, R. *Nat. Chem.* **2011**, *3*, 763.
(17) Goj, A.; Bittner, E. R. *J. Chem. Phys.* **2011**, *134*, 205103.
(18) Yagasaki, T.; Saito, S. *J. Chem. Phys.* **2008**, *128*, 154521.
(19) Jansen, T. L. C.; Knoester, J. *J. Phys. Chem. B* **2006**, *110*, 22910.
(20) Liang, C.; Jansen, T. L. C. *J. Chem. Theory Comput.* **2012**, *8*, 1706.
(21) Torii, H. *J. Phys. Chem. A* **2006**, *110*, 4822.
(22) Redfield, A. G. *Adv. Magn. Reson.* **1965**, *1*, 1.
(23) Kjellberg, P.; Brüggeman, B.; Pullerits, T. *Phys. Rev. B* **2006**, *74*, 024303.
(24) Dijkstra, A. G.; Jansen, T. L. C.; Knoester, J. *J. Chem. Phys.* **2008**, *128*, 164511.
(25) Olbrich, C.; Jansen, T. L. C.; Liebers, J.; Aghtar, M.; Strümpfer, J.; Schulten, K.; Knoester, J.; Kleinekathöfer, U. *J. Phys. Chem. B* **2011**, *115*, 8609−8621.
(26) Jansen, T. L. C.; Cringus, D.; Pshenichnikov, M. S. *J. Phys. Chem. A* **2009**, *113*, 6260.
(27) Roy, S.; Pshenichnikov, M. S.; Jansen, T. L. C. *J. Phys. Chem. B* **2011**, *115*, 5431−5440.
(28) Shi, Q.; Chen, L.; Nan, G.; Xu, R.; Yan, Y. *J. Chem. Phys.* **2009**, *130*, 164518.
(29) Shi, Q.; Geva, E. *J. Chem. Phys.* **2008**, *129*, 124505.
(30) McRobbie, P. L.; Geva, E. *J. Phys. Chem. A* **2009**, *113*, 10425.
(31) Hanna, G.; Geva, E. *J. Phys. Chem. B* **2009**, *113*, 9278.
(32) Kwac, K.; Geva, E. *J. Phys. Chem. B* **2012**, *116*, 2856.
(33) Ishizaki, A.; Tanimura, Y. *J. Phys. Chem. A* **2007**, *111*, 9269.
(34) Kreisbeck, C.; Kramer, T.; Rodriguez, M.; Hein, B. *J. Chem. Theory Comput.* **2011**, *7*, 2166−2174.
(35) Chen, L.; Zheng, R.; Shi, Q.; Yan, Y. *J. Chem. Phys.* **2010**, *132*, 024505.
(36) Palmieri, B.; Abramavicius, D.; Mukamel, S. *J. Chem. Phys.* **2009**, *130*, 204512.
(37) Bastida, A.; Cruz, C.; Zuniga, J.; Requena, A.; Miguel, D. *Chem. Phys. Lett.* **2006**, *417*, 53−57.
(38) Tully, J. C. *J. Chem. Phys.* **1990**, *93*, 1061−1071.
(39) May, V.; Kühn, O. *Charge and energy transfer dynamics in molecular systems*; Wiley-VCH: Berlin, 2000.
(40) Billing, G. D. *The Quantum Classical Theory*; Oxford University Press: New York, 2003.
(41) Schmidt, J. R.; Corcelli, S. A.; Skinner, J. L. *J. Chem. Phys.* **2005**, *123*, 044513.
(42) Parandekar, P. V.; Tully, J. C. *J. Chem. Theo. Comp.* **2006**, *2*, 229−235.
(43) Mukamel, S. *Principles of Nonlinear Optical Spectroscopy*; Oxford University Press: New York, 1995.
(44) Ehrenfest, P. *Z. Phys.* **1927**, *45*, 455−457.
(45) Parandekar, P. V.; Tully, J. C. *J. Chem. Phys.* **2005**, *122*, 094102.
(46) Khalil, M.; Demirdoven, N.; Tokmakoff, A. *J. Phys. Chem. A* **2003**, *107*, 5258−5279.
(47) Tanimura, Y.; Kubo, R. *J. Phys. Soc. Jpn.* **1988**, *58*, 101.
(48) Ishizaki, A.; Fleming, G. R. *J. Chem. Phys.* **2009**, *130*, 234111.
(49) Tempelaar, R.; van der Vegte, C. P.; Knoester, J.; Jansen, T. L. C. in preparation,
(50) Ding, J.-J.; Xu, J.; Hu, J.; Xu, R.-X.; Yan, Y. *J. Chem. Phys.* **2011**, *135*, 164107.
(51) Struempfer, J.; Schulten, K. *J. Chem. Theory Comput.* **2012**, *8*, 2808−2816.